

1    **An experimental-based model for the assessment of the mechanical properties of road**  
2    **pavements using ground-penetrating radar**

3    Fabio TOSTI<sup>1</sup>, Luca BIANCHINI CIAMPOLI<sup>2</sup>, Fabrizio D'AMICO<sup>2</sup>, Amir M. ALANI<sup>1</sup>, Andrea  
4    BENEDETTO<sup>2</sup>

5    <sup>1</sup>School of Computing and Engineering, University of West London (UWL), St Mary's Road,  
6    Ealing, London W5 5RF, UK

7    e-mail: Fabio.Tosti@uwl.ac.uk (\*Corresponding author); Amir.Alani@uwl.ac.uk

8    <sup>2</sup>Department of Engineering, Roma Tre University, Via Vito Volterra 62, 00146, Rome, Italy

9    e-mail: luca.bianchiniciampoli@uniroma3.it; fabrizio.damico@uniroma3.it;

10    andrea.benedetto@uniroma3.it.

11

12    **ABSTRACT**

13    This work proposes an experimental-based model for the assessment of the stiffness of a road  
14    flexible pavement using ground-penetrating radar (GPR – 2 GHz horn antenna) and light falling  
15    weight deflectometer (LFWD) non-destructive testing (NDT) methods. It is known that the  
16    identification of early decay and loss of bearing capacity is a major challenge for effective roads  
17    maintenance and the implementation of pavement management systems (PMS). To this effect, a  
18    time-efficient methodology based on quantitative and qualitative modelling of road stiffness is  
19    developed. The viability of using a GPR system in combination with LFWD equipment is also  
20    proven.

21

22    **Keywords:** ground-penetrating radar (GPR); light falling weight deflectometer (LFWD); non-  
23    destructive testing (NDT); road flexible pavements; road stiffness; health monitoring and

24 assessment; time-efficient methodology; quantitative and qualitative modelling; pavement  
25 management system (PMS).

## 26 1. INTRODUCTION

27 Reducing the number of accidents is a major priority and a challenging target to achieve for road  
28 administrators. Accidents are generally related to geometric issues [1] and unfavourable  
29 serviceability conditions [2]. Firstly, improper design of road geometric elements affects drivers'  
30 perception of the road trajectory. Secondly, low road serviceability levels lead, above all, to lack of  
31 friction between the vehicles and the road surface. With regard to the latter issue, the  
32 intercorrelation between pavement decay and frequency of accidents is well known [3]. To this  
33 effect, an extensive and time-efficient assessment of roads at the network level is crucial for road  
34 administrators and agencies to define priorities of intervention and decrease the likelihood of  
35 envisaged accidents.

36 Most of the damages in flexible pavements occur where the stiffness of the asphalt and load-bearing  
37 layers is low. Therefore, an effective assessment of the strength and deformation properties of these  
38 layers can lead to identifying causes and locating the depth of damages. In addition, a prompt  
39 detection of early decay and loss of bearing capacity represents the real challenge to tackle for road  
40 administrators.

41 It is known that the bearing capacity of subgrade soils can be evaluated by on-site [4, 5] and  
42 laboratory [6] tests. These mainly assess the deformation of the pavement when a constant stress is  
43 applied. Due to the high operational time and costs, these tests are usually carried out on a few road  
44 sections and provide only partial information on the stiffness of the layers. Furthermore, these  
45 methods are intrusive and require to close the highway entirely or partially, with implications for  
46 the driving safety of roads.

47 In view of the above limitations, non-destructive testing (NDT) methods have become popular for  
48 the assessment of the mechanical properties of pavements. Falling weight deflectometer (FWD) [7]  
49 and light falling weight deflectometer (LFWD) [8, 9] are widely used for the investigation of  
50 integrated flexible pavement structures and for construction quality control of unbound materials,  
51 respectively. Nevertheless, LFWD has found also effective application in the assessment of  
52 stiffness of bound layers [10, 11]. The FWD method relies on the measurement of deflections  
53 produced by a known falling mass loading the pavement surface. The main limitation of this  
54 method is that data can be collected only at discrete points, thereby affecting time and cost of the  
55 operations. To fill this gap, fully equipped non-destructive testing lorries for estimation of pavement  
56 strength and deformation properties at traffic speed have been therefore developed. In this regard,  
57 the curviameter [12] uses geophones to measure the velocity of vertical displacements of the  
58 pavement under the passage of the rear axle of the truck. Collection velocity is 18 km/h. The  
59 deflection bowl is obtained by integration of the measurements from the geophones, which are  
60 placed in a chain system. The main limitation of this equipment relates with the integration process.  
61 In this regard, an accurate calibration of the geophones is required. Furthermore, the need to respect  
62 a constant speed and the impossibility to make measurements in curves with radius lower than 40m  
63 are worthy of mention. A traffic speed deflectometer (TSD) [13] is another moving deflectometer.  
64 It operates at speeds up to 90 km/h and it is equipped with a long and rigid beam placed inside a  
65 semi-truck. A dedicated dead weight of 100 kN is located in the proximity of the rear axle. High-  
66 rate sensors, including Doppler sensors, accelerometers and laser distance sensors, ensure that  
67 vertical pavement deflection velocities are recorded. Deflection velocities divided by the  
68 instantaneous vehicle speed produce the deflection slopes at discrete points along the TSD route.  
69 Several internal and external factors may affect the accuracy and precision of TSD measurements.  
70 These include calibration and quality assurance procedures, wind and temperature during the  
71 measurement, pavement roughness and tire-pavement interaction [14]. Although all the  
72 aforementioned methods are reliable and time-efficient, estimation of the strength and deformation

73 properties of pavement layers requires a multi-stage collection of complementary information from  
74 different equipment (e.g., ground-penetrating radar (GPR)). In addition, the integration of this  
75 information requires a repeat of the data collection stage for each equipment along the whole stretch  
76 of the investigated roadway.

77 GPR has been extensively used in highway engineering as a result of the high reliability in the  
78 assessment of the geometric properties and physical properties of the pavement layers. GPR  
79 systems equipped with air-coupled antennas and connected to vehicles are mostly used for data  
80 collection at traffic speed. The GPR working principles rely on the emission of electromagnetic  
81 (EM) waves towards the ground. The emitted waves are then reflected back from the targets  
82 (typically represented by the interfaces of the layers) and are received by a receiving antenna. The  
83 collected signal is therefore displayed and stored for data processing and interpretation purposes. To  
84 date, GPR is successfully utilised in several disciplines including civil engineering [11], demining  
85 [15], archaeology [16], geology [17], glaciology [18] and much more.

86 As a common practice in highway engineering, the GPR and FWD methods are used separately for  
87 the assessment of the geometric (i.e., evaluation of the layer thicknesses) and the strength and  
88 deformation properties (i.e., evaluation of the deflection bowl) of road flexible pavements,  
89 respectively. The integration of the above information allows to evaluate reliable values of stiffness  
90 modulus of the pavement layers.

91 In view of the aforementioned limitations and state-of-the-art practices in the assessment of the  
92 mechanical properties of flexible pavements, the development of a non-destructive testing  
93 methodology for real-time identification of early decay and loss of bearing capacity of roads at  
94 traffic speed would stand as a step forward compared with the traditional methods. Value added  
95 would be to provide an estimation of the pavement stiffness based on geometric, physical and  
96 mechanical attributes of the subsurface integrated into a unique model. This would emphasize  
97 strengths and narrow weaknesses of the above NDTs.

98 A first modelling approach was developed by Tosti et al. [19]. A ground-coupled GPR antenna  
99 system and LFWD equipment were used to collect a dense dataset on a flexible pavement structure.  
100 The model was based on the peak amplitudes of the GPR signals reflected at the interfaces of the  
101 road layers and the stiffness moduli estimated using LFWD. The concept proposed by Tosti et al.  
102 [19] is here taken as a reference and it is further developed using an air-coupled GPR antenna  
103 system.

104 It is important to emphasize the importance of the proposed methodology in assessing early decay  
105 and loss of bearing capacity of the load bearing layers more efficiently than the state-of-the-art  
106 NDT methods. This information would be crucial for road administrators in order to create  
107 comprehensive databases of the road pavement conditions at the network level for implementation  
108 in pavement management systems (PMSs). This would allow for prioritisation of road maintenance  
109 operations, reduction of costs and a decrease in the likelihood of envisaged accidents.

110 The paper is outlined as follows: in Section 2, the aim and objectives are presented. The theoretical  
111 framework is discussed in Section 3. Section 4 presents the methodology, whereas the experimental  
112 design (test site and equipment) is detailed in Section 5. The ground-truth information and the  
113 preliminary data analysis are discussed in Section 6. The modelling is presented in Section 7,  
114 whereas results and discussion are reported in Section 8. Finally, the conclusion and future  
115 prospects are discussed in Section 9.

## 116 117 2. AIM AND OBJECTIVES

118 The primary aim of this project is to address a major challenge in the identification of early decay  
119 and loss of bearing capacity in road flexible pavements using GPR and LFWD. To achieve this aim,  
120 the following objectives are set:

- 121 • to develop a time-efficient methodology for estimating the stiffness of the pavement structure;
- 122 • to demonstrate the viability of using an air-coupled GPR antenna system in combination with  
123 LFWD equipment.

124  
125

### 3. THEORETICAL FRAMEWORK

126 The GPR method is based on the theory of the EM fields. When an EM wave is emitted by a  
127 source, propagation is ruled by the dielectric properties of the medium that is passed through (case  
128 of non-magnetic targets). In more detail, propagation speed and attenuation of the wave are related  
129 to the relative dielectric permittivity  $\epsilon_r$  [-] and the electrical conductivity  $\sigma$  [ $\text{Sm}^{-1}$ ], respectively.  
130 When a dielectric discontinuity is encountered, the radiated energy is partly reflected back to the  
131 receiving antenna and partly transmitted in depth. From the analysis of the collected signal, it is  
132 therefore possible to reconstruct the geometric features of the discontinuities.

133 Within this framework, the volumetric content of air and water that fills the inter-particle voids of  
134 pavement materials highly influences the dielectrics of the road pavement layers. However,  
135 compaction conditions of the pavement layers are also highly dependent on the content of inter-  
136 particle voids in construction materials. Hence, it is reasonable to assume that compaction of  
137 pavement materials may affect the EM behaviour of the layers [20]. With regards to the load-  
138 bearing layers and subgrade soils, it is also worth mentioning that soil particle compaction is highly  
139 dependent on their grain size distribution. This affects, in turn, the number of contacts between the  
140 grains and, hence, the shear strength of the material (along with the particle mineralogy and  
141 roughness) [21]. To this effect, compaction is performed on site after the laying out of loose soil  
142 granular materials. This allows to activate frictional resistance and interlocking of grains in order to  
143 reach a higher bearing capacity.

144 The strength of bearing soils in unsaturated conditions is also highly dependent on the physical state  
145 of water within the inter-particle voids. In this regard, it is known that free water can create  
146 differing physical-chemical bonds as a function of both size and type of soil particles. These bonds  
147 affect the cohesion between particles and, hence, the bearing capacity of subgrades. According to  
148 Mitchell [22], the dielectric properties of materials (e.g., dielectric loss and permittivity) are also  
149 dependent on the aforementioned inter-molecular bonds. Furthermore, Carpenter et al. [23]

150 demonstrated how several pavement damages visible on the surface, such as transverse cracking,  
151 are caused by freeze-thaw cycling affecting the whole pavement structure. Indeed, this process  
152 induces a seasonal volumetric contraction and dilation of the unbound layers and, mostly, the base  
153 layer. More recently, Scullion and Saarenketo [24] also proved the high correlation between the  
154 thermal susceptibility and the water suction in unbound bearing soils. Changes in the dielectric  
155 behaviour of soils were also found to be highly related to water suction effects.

156 In view of the aforementioned research, it is likely to expect a relationship between the dielectric  
157 and the strength and deformation properties of the unbound materials of road pavements [25, 26].

158 A road flexible pavement is generally described as a multi-layer structure composed of hot-mixed  
159 asphalt (HMA) bitumen-bound layers overlaying unbound granular courses. This structure is laid  
160 over a bearing subgrade [27]. It is known that the bond of the shallowest road layers is due to the  
161 high shear stresses transferred by the moving vehicles at the wheel-surface contact. Conversely,  
162 unbound granular materials are used for the construction of the foundation layers. These latter along  
163 with the subgrade soil receive stress generation from the above layers and bear the major structural  
164 contribution in terms of loads [28].

165 By considering a flexible pavement as a simplified homogenous half-space, the stress distribution  
166 with depth can be described using the theory of Boussinesq [e.g., 29] and its generalization to multi-  
167 layer configurations [30]. To this effect, the graphical solutions proposed by Forster and Ahlvin  
168 [31], clearly show that in the surroundings of a bearing area with a radius equal to 15 cm (e.g., case  
169 of a common lorry), most of the vertical stress concentrates beyond 7 cm of depth. This depth is  
170 typically out of the thickness of an HMA layer. This occurrence was also proved using numerical  
171 simulation [32]. Hence, it can be argued that loosely bound and unbound granular layers (especially  
172 the base layer) may heavily affect the mechanical behaviour of the whole road pavement structure.  
173 To this purpose, it is worth mentioning the research work of Scullion and Saarenkeeto [24]. The  
174 authors observed volumetric shrinkage caused by freezing in several base layers of different road

flexible pavements. These contractions were one order of magnitude greater than shrinkage measured in the asphalt layers and were observed to cause cracking at the surface. Furthermore, structural rutting was investigated by Oteng-Seifah and Manke [33] and Simpson et al. [34] and was related to deformations located in the base layer and the subgrade.

In view of the research studies above, it can be argued how thickness and development of the base layer may affect the bearing capacity of a whole pavement structure.

Further to the aforementioned geometric factors, it is known how the bearing capacity of flexible pavements may be highly affected by critical physical attributes [35], such as the content of clay. The upward passage of the smallest clay slurry particles from the subgrade by capillary actions lowers the strength and deformation properties of the pavement structure. To this effect, the correlation between clay content and plastic deformation of soils under load has been widely investigated in the literature [22]. From an EM standpoint, the viability of using GPR for detection of clay in dry and saturated soils has been demonstrated. As the applied EM field is affected by the presence of clay in a medium, relevant information can be estimated from the collected signal (in both the time and the frequency domain) [36, 37]. Attenuation of the EM waves is one of the most easily detectable effects related to the presence of clay in soils. In the case of dielectric materials, signal attenuation can be expressed by the propagation loss  $L = \exp\{-bz\}$  [38], with  $b$  being the attenuation coefficient and  $z$  being the investigation depth. The coefficient  $b$  is highly dependent on the electric conductivity of the medium  $\sigma$  [ $\text{Sm}^{-1}$ ]. As clayey soils are typically characterised by high values of  $\sigma$  (mostly in wet conditions), then clay presence can be related to greater attenuations of the EM wave. In view of this, it can be argued that the amplitude of the received GPR signals is likely affected by the upward passage of clayey slurry particles towards the shallowest layers of a road flexible pavement.

198

#### 199 4. METHODOLOGY



200 The study focuses on the estimation of the stiffness of a road flexible pavement whereby a unique  
201 modulus for the overall pavement strength is considered. To this purpose, experimental tests are  
202 carried out using an air-coupled GPR antenna system and LFWD equipment.

203 Outliers are first filtered out from the LFWD dataset along with the relative GPR signals. A  
204 parametric model is therefore developed. In this regard, LFWD data are used as ground-truth  
205 measurements of pavement stiffness for modelling purposes. On the other hand, GPR data provide  
206 geometric and physical attributes about the pavement structure. The model parameters are first  
207 calibrated against the ~10% of data from the full dataset. A quantitative validation of the model  
208 viability is therefore carried out across the full road stretch length. Based on these outcomes, a  
209 qualitative approach for the estimation of the pavement stiffness is also developed.

## 210

### 211 5. EXPERIMENTAL DESIGN: TEST SITE AND EQUIPMENT

212 Experimental tests are carried out in the District of Rieti, Italy. To this purpose, 1500 m of a two-  
213 lane highway (one lane per direction) with a flexible pavement structure are investigated using GPR  
214 and LFWD equipment. From the available design drawings of the pavement structure, the  
215 superstructure is made of a 0.05-m-thick surface layer, a 0.10-m-thick bitumen-bond base layer and  
216 a 0.30-m-thick subbase layer (unbound granular material).

217 With regard to the GPR equipment, the RIS Hi-Pave HR1 2000 air-coupled antenna system,  
218 manufactured by IDS Georadar, is used. The system is equipped with a mono-static antenna of 2  
219 GHz central frequency, mounted behind an instrumented van. The high frequency of investigation  
220 and type of antenna system allow to collect reflections of the GPR signal from the interfaces  
221 between the thinner surface layers as well as to perform the investigation at traffic speed. Traces are  
222 collected every 0.027 m to allow further statistical analyses about the optimal horizontal sampling  
223 resolution.

224 Tests for the collection of ground-truth data of pavement stiffness are carried out using the LFWD

Prima 100 manufactured by Carl Bro Pavement Consultants Kolding. The equipment is composed of a circular metal plate (diameter 100 mm) loaded by a 10 kg hammer and a set of geophones that allow to record the pavement deflections  $\delta_c$  [ $\mu\text{m}$ ]. The LFWD investigation points are spaced 10 m from one another so that 151 points are collected along the investigated road stretch. It is worth noting that LFWD is a less acknowledged piece of testing equipment than the FWD for the investigation of the stiffness of bound layers. Nevertheless, LFWD is used in this study for calibration and validation purposes for consistency with past research on GPR [19] and LFWD [9, 10] as well as to foster the time-efficiency of the proposed methodology.

233

## 6. GROUND-TRUTH INFORMATION AND PRELIMINARY DATA ANALYSIS

An “equipollent” modulus of stiffness  $E_{MEA,x}$  at a generic position  $x$  (corresponding to a generic load point) is calculated implementing the deflections from LFWD in the Boussinesq solution [e.g., 29] as follows [39]:

$$E_{MEA,x} = \frac{k(1-\nu^2)\sigma_x R}{\delta_{c,x}} \quad (1)$$

where  $k$  is a constant equal to 2 (case of flexible pavements),  $\nu$  [-] is the Poisson ratio,  $\sigma_x$  [MPa] is the load stress,  $R$  [mm] is the plate radius and  $\delta_{c,x}$  [ $\mu\text{m}$ ] is the deflection measured at the center of the LFWD plate. A number of 6 loading tests were performed at each survey point to ensure statistically significant data outputs [8]. Correction of the estimated stiffness due to temperature effects is not applied to the LFWD data, as the test conditions are close to the benchmark temperature suggested in the literature [40].

The use of LFWD deals satisfactorily with the model outline discussed above, as the expected maximum depth of the bottom of the base layer is, by design drawings, around 15 cm. This depth matches well the maximum depth of the deflection basin expected for this equipment in road pavement investigations [9]. From now on, values of  $E_{MEA,x}$  estimated by Eq. (1) will be used as

249 ground-truth data for modelling purposes. This parameter will be referred to as “measured stiffness  
250 modulus”  $E_{MEA,x}$  at a generic position  $x$ .

251 Each dataset of 6 LFWD measurements collected at the 151 investigation points along the “full”  
252 road stretch length  $l_{tot}$  is processed in terms of force applied, vertical stress and deflections. Datasets  
253 with low statistical significance [9] are discarded in full and the relative investigation points are  
254 removed from the statistical population. In view of this, the relevant LFWD investigation points are  
255 reduced from 151 to 120 so that a 1200m-long road stretch (from now on referred to as “processed  
256 road stretch”  $l_{proc}$ ) is considered for modelling purposes. The related GPR traces are also  
257 consistently filtered out from the GPR dataset. A standard processing scheme for road inspections is  
258 applied to the GPR data [41]. In this regard, the zero-offset removal, the bandpass filtering and the  
259 cut-off of the air layer are applied.

## 260 261 7. MODELLING

### 262 7.1 Model outline

263 An experimental-based parametric model for the estimation of the stiffness of road flexible  
264 pavements is developed. Strength and deformation properties of a road flexible pavement at a  
265 generic position  $x$  are expressed, in terms of stiffness modulus  $E'_{MOD,x}$  [MPa], as follows:

$$266 \quad E'_{MOD,x} = \alpha(E_{MOD,x}) E_{MOD,x} \quad (2)$$

267 with  $\alpha(E_{MOD,x})$  being a fitting function and  $E_{MOD,x}$  [MPa] being a first approximation stiffness  
268 modulus. This latter parameter is defined as follows:

$$269 \quad E_{MOD,x} = \tau_{b,x} \beta_x \gamma_x \quad (3)$$

270 where  $\tau_{b,x}$  [m] accounts for the thickness of the base layer,  $\beta_x$  [MPa m<sup>-1</sup>] is a scale factor and  $\gamma_x$  [-]  
271 takes into account the contribution of clay to the stiffness modulus.

272 The modelled stiffness modulus  $E'_{MOD,x}$  in Eq. (2) is estimated through calibration of the  $\alpha(E_{MOD,x})$   
 273 fitting function and the relative first approximation stiffness modulus  $E_{MOD,x}$  (Eq. (3)). This latter  
 274 requires in turn calibration of the  $\beta_x$  and  $\gamma_x$  parameters, whereas  $\tau_{b,x}$  is a constant value taken from  
 275 the trend of the base layer thickness. Calibration of the above parameters is carried out over a  
 276 100m-long distance within the 1200m-long processed road stretch  $l_{proc}$ .

277

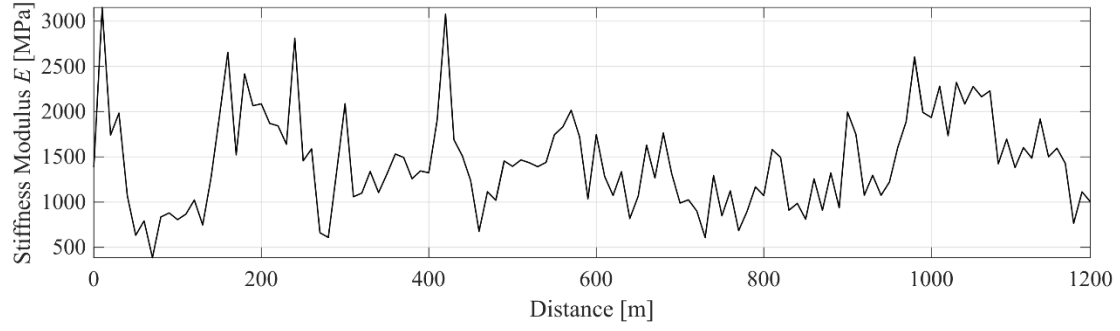
## 278 **7.2 Evaluation of the base layer thickness**

279 The thickness of the base layer  $\tau_{b,x}$  is assessed with reference to the two-way travel time (TWTT)  
 280 distance covered by the GPR signal to pass through the concerning layer [42]. The value of this  
 281 parameter at a generic position  $x$  is calculated as follows:

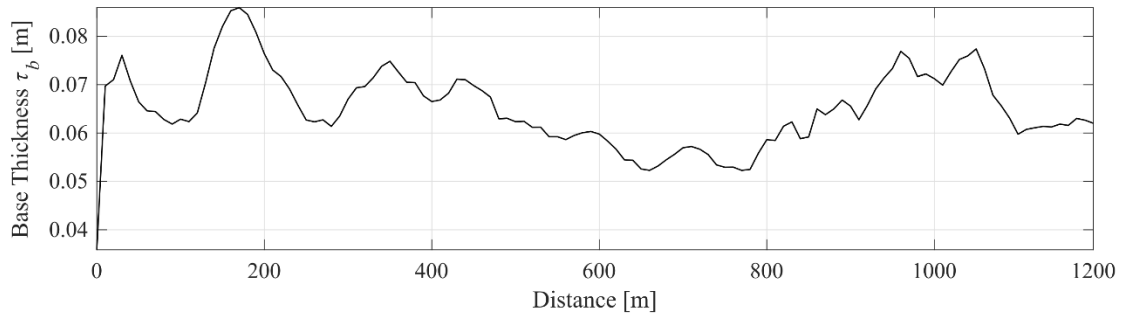
$$282 \quad \tau_{b,x} = \frac{c \Delta t_x}{2\sqrt{\epsilon_{r,b,x}}} \quad (4)$$

283 where  $c$  [ $\text{ms}^{-1}$ ] is the wave velocity of propagation in the free space,  $\Delta t_x$  [s] is the temporal distance  
 284 between the reflection amplitude peaks of the top and the bottom of the base layer (i.e., the peak-to-  
 285 peak time distance), and  $\epsilon_{r,b,x}$  [-] is the relative dielectric permittivity of the material passed through  
 286 within the base layer.

287 Fig. 1 depicts a comparison between trends of measured stiffness modulus  $E_{MEA,x}$  (Fig. 1(a)) and  
 288 base layer thickness  $\tau_{b,x}$  (Fig. 1(b)). The similarity between the two trends is shown; hence, a  
 289 correlation between these two parameters could be likely deemed.



(a)



(b)

**Fig. 1.** Comparison between trends of (a) measured stiffness modulus (LFWD – Eq. (1)) and (b) base layer thickness (GPR – Eq. (4)).

### 7.3 Model calibration

A 100 m-long section ( $l_{cal}$ ), located between markers 170 m and 270 m of the processed road stretch  $l_{proc}$ , is randomly selected for calibration purposes. This distance represents the 6.7% and the 8.3% of the "full" ( $l_{tot} = 1500$  m) and the "processed" ( $l_{proc} = 1200$  m) road stretch lengths, respectively.

It is worth noting that the outcomes of the calibration process discussed hereafter are representative of the specific testing conditions of this study. These include the flexible pavement structure described in Section 5 and the percentage of ground-truth data of pavement stiffness taken for calibration purposes. Hence, other values of the calibration parameters apply in the case of different boundary conditions.

#### 7.3.1 Dimensional scaling

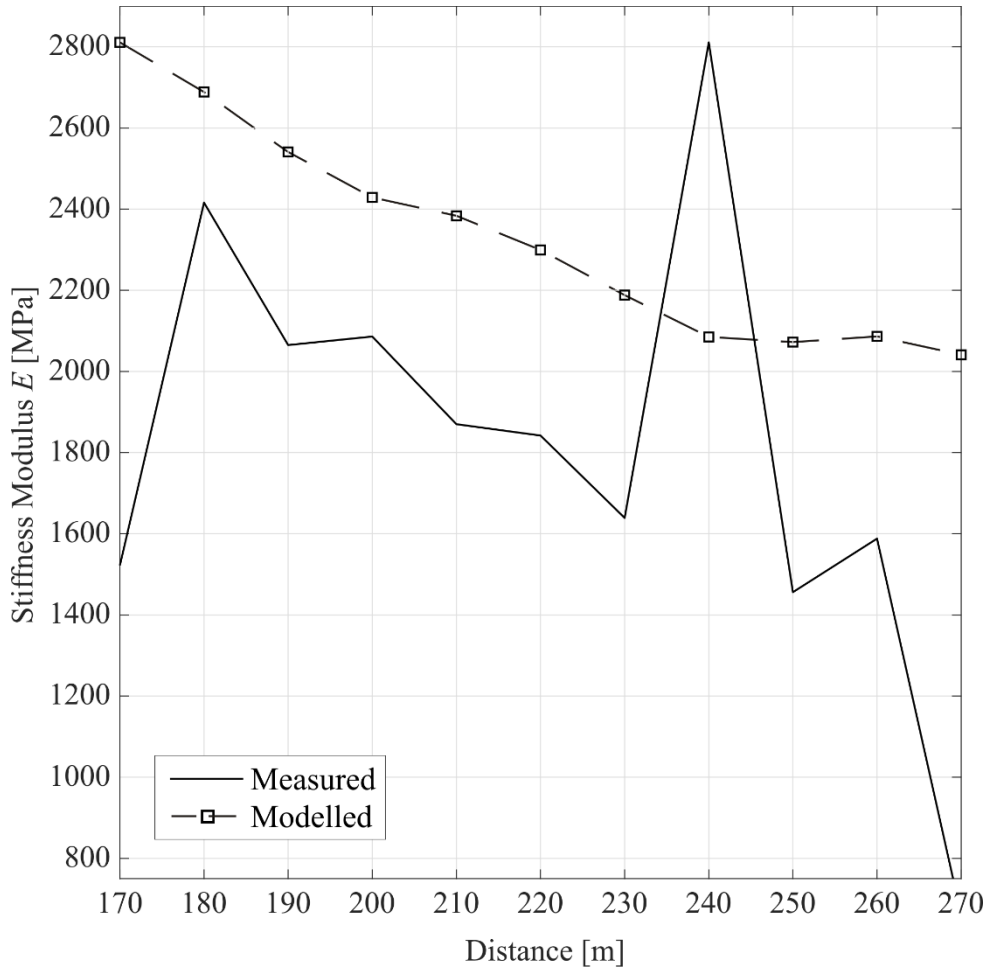
305 The scale factor  $\beta_x$  is set as:

$$306 \quad \beta_x = \frac{E_{MEA,x,MAX[l_{proc}]}}{\tau_{b,x,MAX[l_{cal}]}} \quad (5)$$

307 where  $E_{MEA,x,MAX[l_{proc}]}$  is the maximum value of stiffness modulus estimated throughout the 120  
 308 investigation points within the processed distance  $l_{proc} = 1200$  m using Eq. (1), and  $\tau_{b,x,MAX}$  is the  
 309 maximum thickness of the base layer calculated using Eq. (4) within the randomly selected  
 310 calibration road stretch  $l_{cal}$ .

311 Fig. 2 shows the trend of preliminarily modelled stiffness modulus  $E_{MOD,x}^* = \beta_x \tau_{b,x}$  along the  
 312 calibration road stretch. It can be seen how the preliminary application of the model generally tends  
 313 to overestimate the measured ground-truth data. This mismatch is further addressed in Section 7.3.3  
 314 using a dedicated fitting function.

315



316

317 **Fig. 2.** Comparison between trends of measured (solid line) and preliminarily modelled (dashed line  
 318 with square markers) stiffness modulus along the 100m-long calibration road stretch.

319

### 320 7.3.2 Clay contribution

321 The amplitude of the central peak of the frequency spectrum  $A_p$  is considered as the benchmark  
 322 parameter to account for the presence of clay rising from the foundation level [27, 28]. To this  
 323 purpose, geological maps of the site [43] are analysed and the investigated stretch of road is  
 324 classified as belonging to a poorly-clayey geological area. Hence, highly attenuated frequency  
 325 spectra are interpreted as indicators of likely presence of clay and are related to areas of early decay  
 326 and loss of road bearing capacity. On the contrary, standard frequency spectra are interpreted as  
 327 indicators of stability in terms of strength and deformation properties of the pavement.

328 The stair function  $\gamma(A_{p,x})$  is defined from the analysis of the central peak amplitude  $A_{p,x}$  of the  
 329 frequency spectrum of the GPR signal collected at a generic position  $x$  within the calibration road  
 330 stretch  $l_{cal}$ . This function is developed to lower the modelled stiffness modulus when the value of  
 331  $A_{p,x}$  is lower than a reference optimal threshold value (i.e., when the spectrum is attenuated). It is  
 332 expressed as follows:

$$333 \quad \gamma(A_{p,x}) = \begin{cases} 0.80 & \text{if } A_{p,x}^{[0,1]} < A_t \\ 1 & \text{otherwise} \end{cases} \quad (6)$$

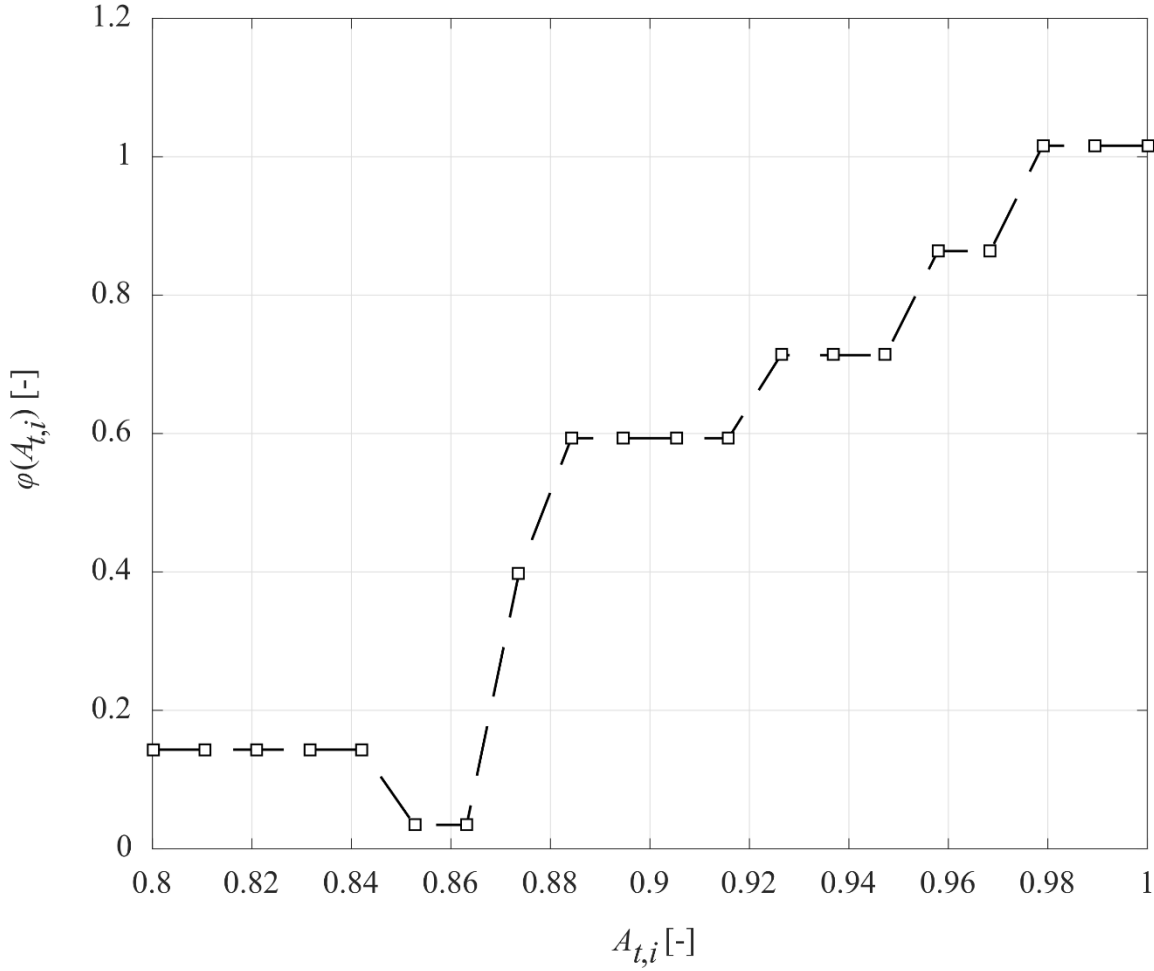
334 where  $A_{p,x}^{[0,1]}$  is the central peak amplitude of the frequency spectrum, normalised in the calibration  
 335 range  $l_{cal}$  and  $A_t$  is the set threshold. The threshold  $A_t$  is defined after running the model for each  $i^{th}$   
 336 value  $A_{t,i}$ , with  $i$  ranging between 0.80 and 1 at steps of 0.01. The trend of the  $i^{th}$  values of  $A_{t,i}$  in the  
 337 defined range is described by the following objective function  $\varphi(A_{t,i})$ :

$$338 \quad \varphi(A_{t,i}) = \sqrt{\frac{\sum_{x=0}^{l_{cal}} |E_{MOD,x,A_{t,i}} - E_{MEA,x}|^2}{\sum_{x=0}^{l_{cal}} E_{MOD,x,A_{t,i}}^2}} \quad (7)$$

339 expressing the mismatch between the modelled ( $E_{MOD,x,A_{t,i}}$ ) and the measured ( $E_{MEA,x}$ ) stiffness

340 modulus. Fig. 3 shows the performance of the model with varying values of  $A_{t,i}$ . A minimum value  
 341 of 0.034 for  $\varphi(A_{t,i})$  is reached when  $A_{t,i}$  is equal to 0.857; hence, this value is taken as the optimal  
 342 threshold expressing  $A_t$ .

343



344

345 **Fig. 3.** The trend of the objective function  $\varphi(A_{t,i})$  with varying values of  $A_{t,i}$ .

346

347 It is worth specifying that the  $\chi(A_{p,x})$  parameter improves the model matching at the local maximum  
 348 and minimum points of the measured trend of stiffness, whereas the overall model overestimation is  
 349 addressed using a dedicated fitting function, as detailed further in Section 7.3.3.

350

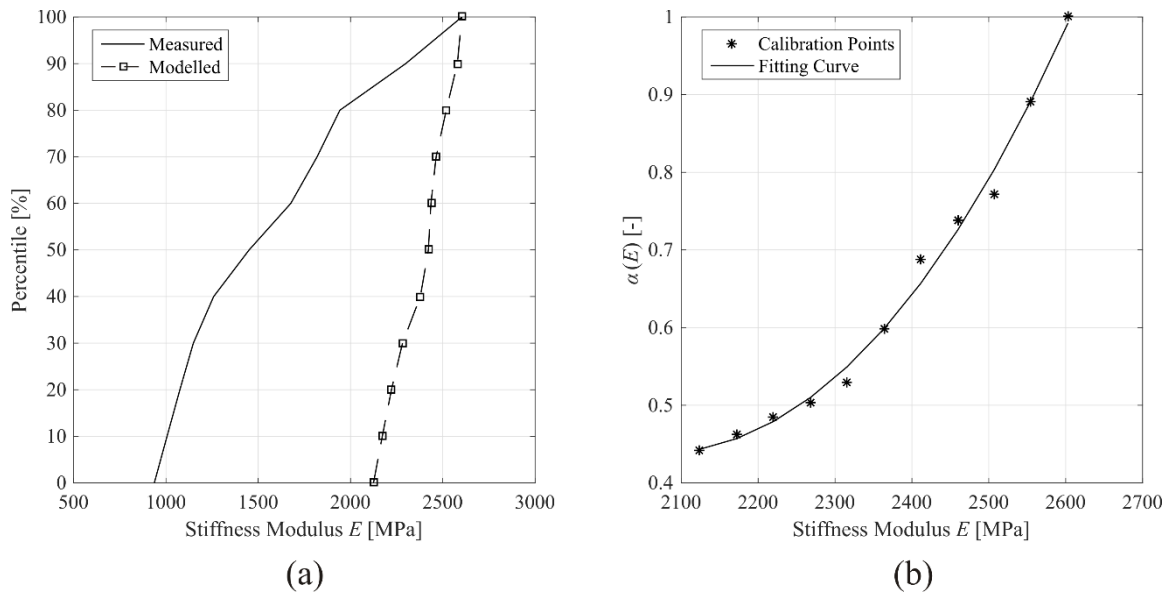
### 351 7.3.3 The fitting function



352 A percentile analysis of measured and modelled stiffness moduli (Fig. 4(a)) is performed to ensure  
 353 accurate evaluation of the model overestimation. The ratio of the modelled to the measured  
 354 percentiles (Fig. 4(b)) is therefore calculated as a reductive factor for compensation purposes.  
 355 Hence, the continuous function  $\alpha(E_{MOD,x})$  is derived using the following third-degree polynomial  
 356 fitting relationship:

$$357 \quad \alpha(E_{MOD,x}) = \sum_{i=0}^3 a_i E_{MOD,x}^i \quad (8)$$

358 The values of the fitting parameters  $a_i$  are reported in Table 1.  
 359



360 (a) Percentile analysis of measured (solid line) and modelled (dashed line with square  
 361 markers) stiffness moduli; (b) fitting function  $\alpha(E_{MOD,x})$  expressed by Eq. (8).  
 362

363  
 364 Table 1 – Fitting parameters  $a_i$  in Eq. (8).

$a_0$	$a_1$	$a_2$	$a_3$
-22.618	0.027	$-1.24 \times 10^{-6}$	$1.74 \times 10^{-9}$

365  
 366 The adjusted modelled trend of stiffness modulus is therefore derived working out the value of the  
 367 fitting function  $\alpha(E_{MOD,x})$  from Eq. (8) into Eq. (2). Figure 5 shows the comparison between trends  
 368 of measured and (adjusted) modelled stiffness modulus along the calibration road stretch.

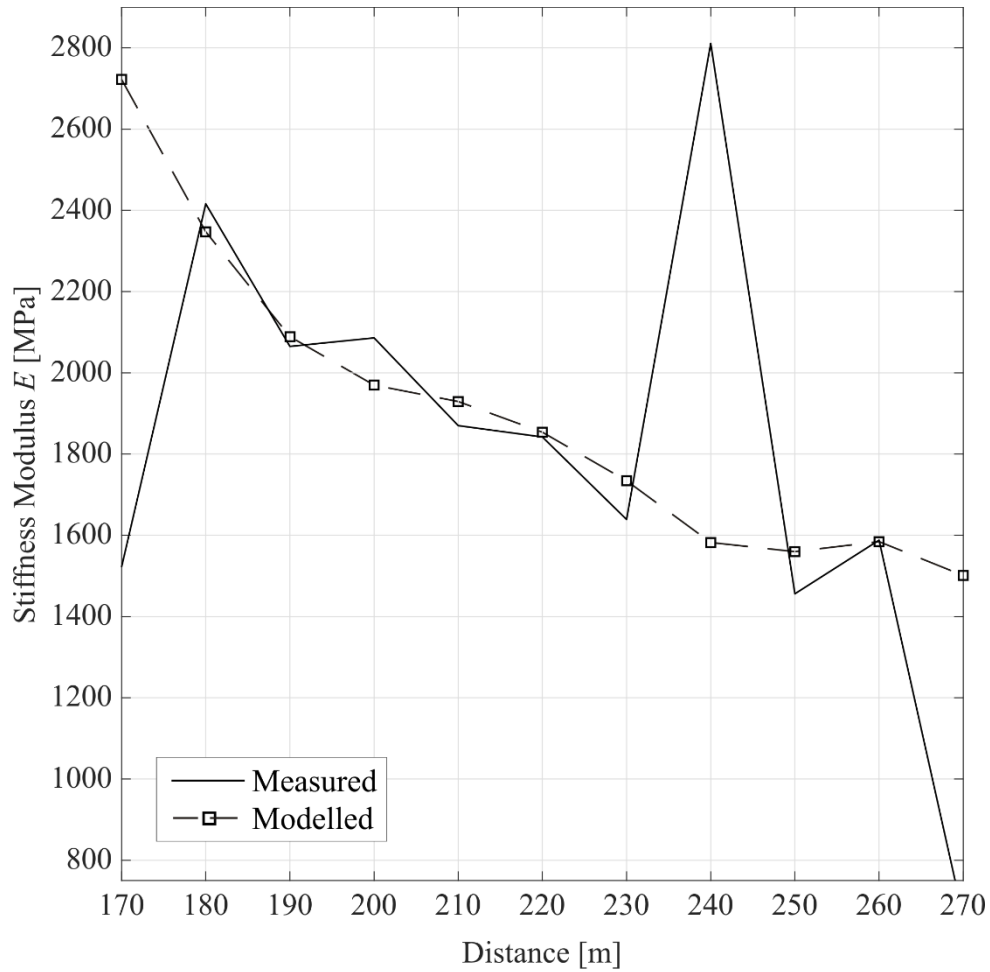
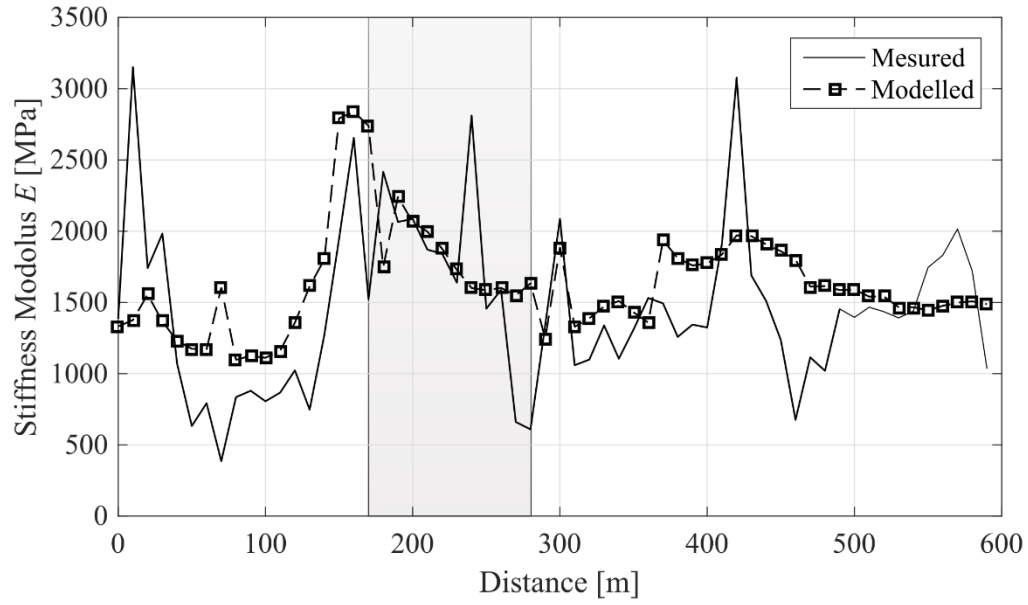


**Fig. 5.** Comparison between trends of measured (solid line) and modelled (dashed line with square markers) stiffness modulus after the application of the fitting function  $\alpha(E_{MOD,x})$  (Eq. (8)).

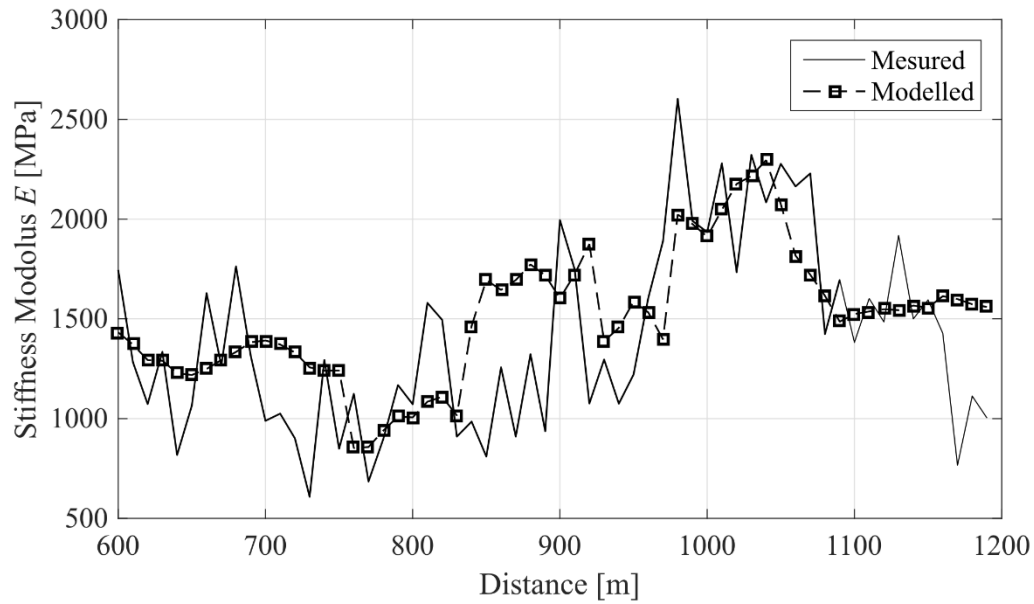
## 8. RESULTS AND DISCUSSION

### 8.1. Validation of the quantitative model

The trend of modelled values of fully-calibrated stiffness modulus  $E'_{MOD,x}$  is estimated along the processed road stretch length  $l_{tot}$ . An overall comparison between trends of measured and modelled stiffness modulus is shown in Fig. 6. For the sake of clarity with the data interpretation, the 1200 m road stretch length is divided into two sub-areas, i.e., from markers “0 m to 600 m” and “600 m to 1200 m”. The area related to the calibration road stretch is marked in grey.



(a)



(b)

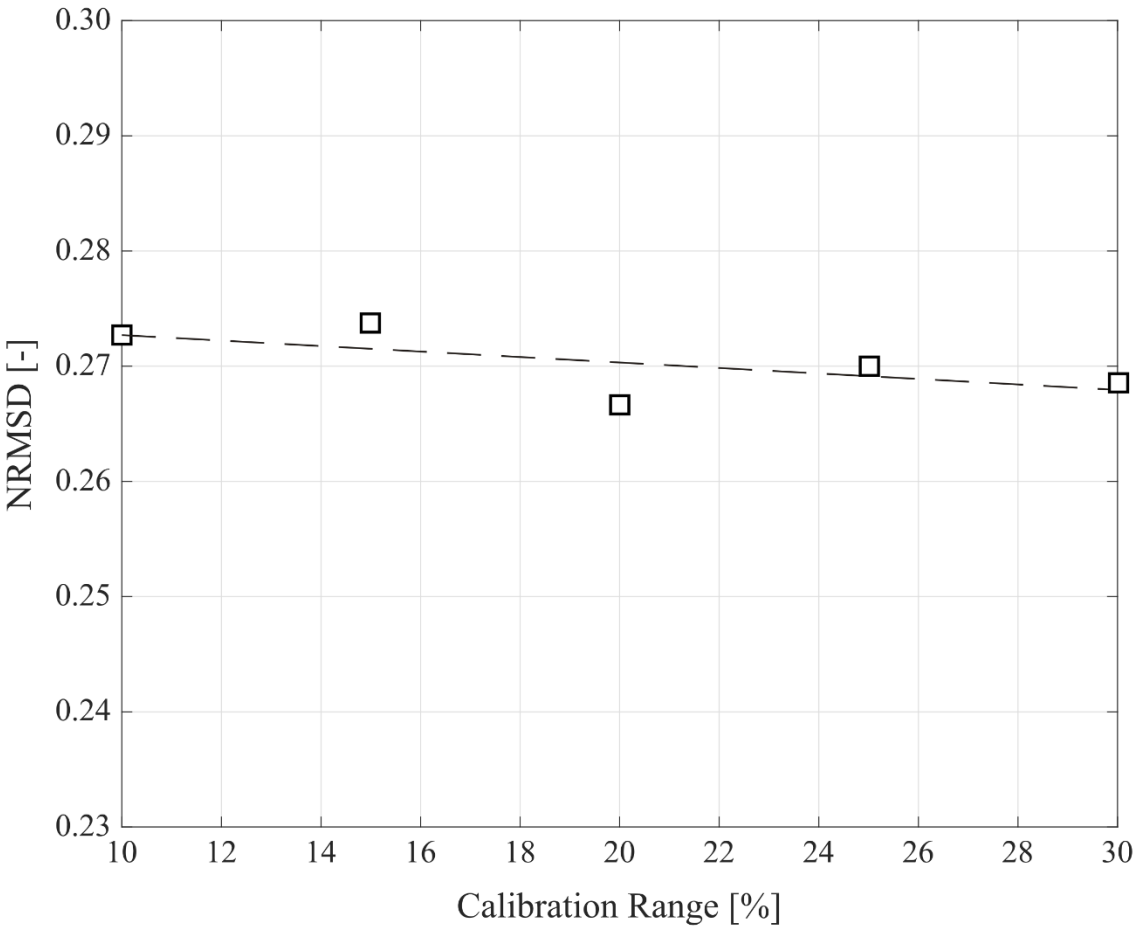
380

381

382 **Fig. 6.** Comparison between trends of measured  $E_{MEA,x}$  (solid line) and modelled  $E'_{MOD,x}$  (dashed  
 383 line with square markers) stiffness modulus after the application of the fully-calibrated model. The  
 384 area related to the calibration road stretch is marked in grey. (a) Markers “0 m – 600 m”; (b)  
 385 markers “600 m – 1200 m”.

386

387 A relatively good reliability of the model for the interpretation of the actual road pavement stiffness  
 388 is proven. A few areas of ground-truth data misinterpretation from the model are still recognizable  
 389 in the neighbourhood of markers “100 m”, “400 m”, “550 m” (Fig. 6(a)) and “900 m” (Fig. 6(b)).  
 390 The normalised root-mean-square deviation (NRMSD) is equal to 0.273. This provides a  
 391 quantitative measurement of disagreement between measured and modelled datasets of stiffness  
 392 modulus.  
 393 The assumption made on the percentage size of the LFWF calibration points (i.e., ~10% of the data  
 394 from the full dataset) is further investigated to verify the robustness of the model. To this purpose,  
 395 the fully-calibrated model is applied with calibration data ranges comprised between 10% and 30%  
 396 in steps of 5%; hence the relative values of NRMSD are found and plotted (Fig. (7)).



397  
 398 **Fig. 7.** The trend of NRMSD values of the model against the percentage range “10% - 30%” of

399 LFWD calibration points.

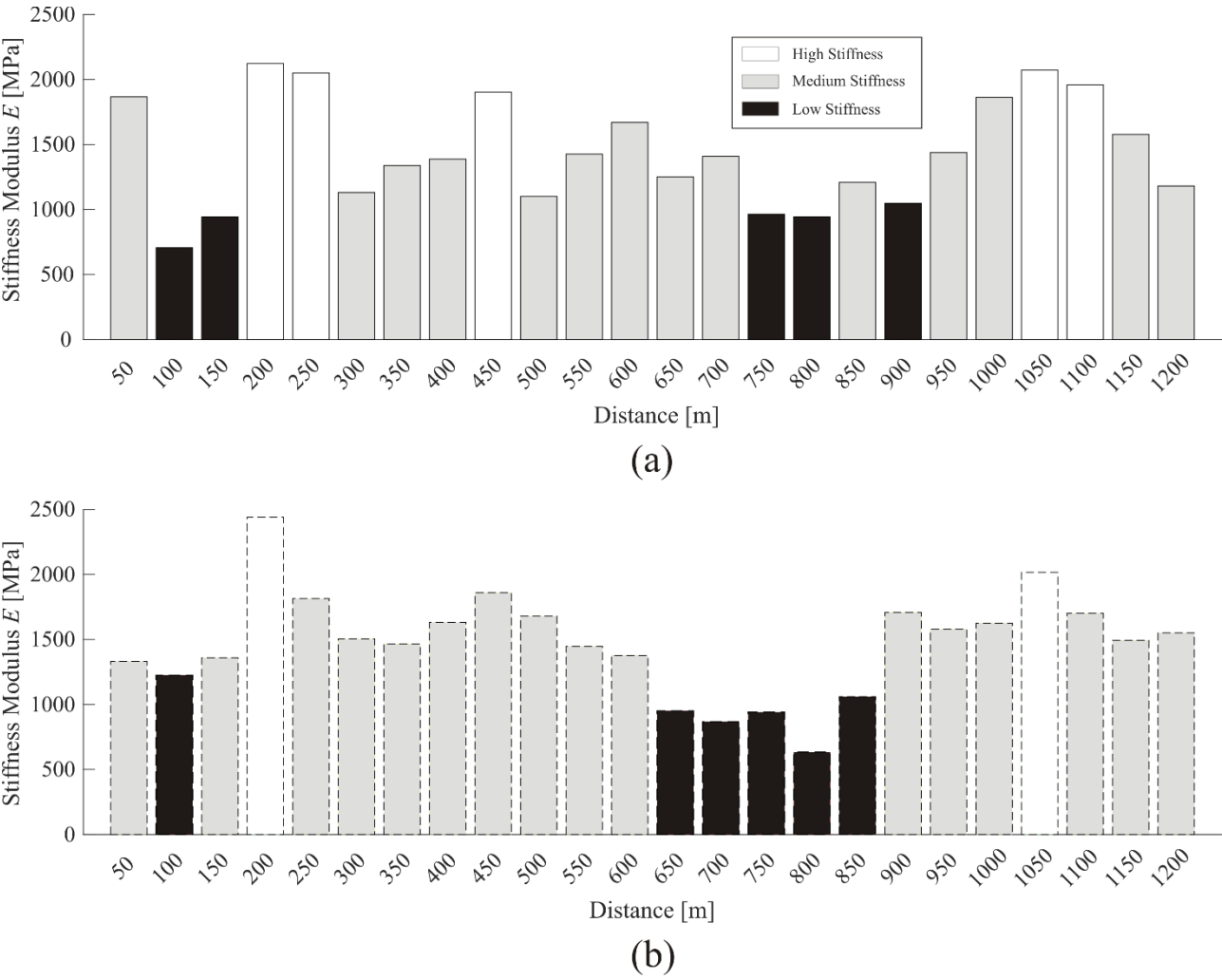
400 It is worth noting how the robustness of the model has a weak dependence on the percentage range  
401 of calibration points. This is proved by the slight variability of the NRMSD values and the fair  
402 horizontality of the least square fitting trend line. Thereby, it is possible to argue that a robust  
403 calibration can be performed using ~10% of ground-truth calibration points, whereas the length of  
404 the relative full dataset is at least the same as the length of the road stretch investigated in this  
405 study. This may represent an invaluable outcome for the development of a more time-efficient  
406 methodology for the estimation of the stiffness of road flexible pavements. In fact, the use of FWD  
407 could be potentially limited to the ~10% only of the full length of the roadway whereas the rest of  
408 the survey could be carried out using an air-coupled GPR system for a more time-efficient data  
409 collection.

410

## 411 **8.2 Qualitative modelling of road pavement stiffness**

412 To foster the viability of using air-coupled GPR antenna systems in combination with FWD  
413 systems in PMSs, a qualitative and streamlined approach to estimate stiffness of road flexible  
414 pavements is further proposed. The rationale behind this process is to provide rapid identification of  
415 early decay and loss of bearing capacity areas at the network level. Hence, time and cost of further  
416 and more detailed investigations can be planned and allocated more effectively.

417 Stiffness moduli estimated from Eq. (1) and Eq. (2) are here considered as ground-truth and  
418 modelled values, respectively. The investigated road stretch is divided into 50m-long value ranges  
419 of stiffness modulus wherein the average value is taken as a benchmark. Three classes of stiffness  
420 are therefore identified, i.e., “high stiffness”, “medium stiffness” and “low stiffness” classes. These  
421 are set as a function of two thresholds, arbitrarily fixed at 1900 MPa and 1100 MPa, according to  
422 the overall trend of modelled stiffness moduli. This step allows for customisation of the  
423 methodology as per the specific requirements of the survey. Fig. (8) shows the outcomes of the  
424 qualitative modelling.



427 **Fig. 8.** Comparison between the three qualitative classes of stiffness modulus: (a) measured  
428 stiffness modulus (bar charts with solid contour lines); (b) modelled stiffness modulus (bar charts  
429 with dashed contour lines).  
430

431  
432 From the comparison between measured and modelled stiffness by the qualitative approach,  
433 matches of two main areas of lowest stiffness are observed in the value ranges “100 m – 150 m”  
434 and “700 m – 900 m”. In addition, a good match between highest stiffness moduli is noticed in the  
435 value ranges “200 m – 250 m” and “1050 m – 1100 m”. The remaining intervals match well with  
436 intermediate stiffness conditions of the road pavement.

437 It is worth noting the relative range of applicability of the proposed approach. The set values of the

threshold are specific to the dataset collected in this investigation. Hence, they may change for a different dataset (e.g., the same pavement structure at a different life cycle stage or another road pavement with a different cross section and/or construction materials). To this effect, the proposed methodology is reliable and can be used to investigate other road flexible pavements only if suitable threshold values are set after a preliminary data analysis at the network level.

## 9. CONCLUSION AND FUTURE PROSPECTS

This work proposes an experimental-based model for the assessment of stiffness in a road flexible pavement using ground-penetrating radar (GPR) and light falling weight deflectometer (LFWD). The model uses ground-truth data of road stiffness inferred from LFWD as well as geometric and physical information of the pavement structure derived from a GPR system equipped with a 2 GHz horn antenna.

To this purpose, 1500 m of a two-lane highway (one lane per direction) with a flexible pavement structure are investigated. After filtering out the outliers from the collected LFWD data (and the relative GPR traces), the model is calibrated via an optimisation process using the ground-truth stiffness moduli at the investigation points of a randomly-selected 100m-long road stretch (i.e., ~10% of the processed dataset), the thickness of the base layer and the central-peak amplitudes of the frequency spectrum. These latter parameters are both estimated using GPR and account for the structural quality of the pavement and the clay content in the load-bearing layers, respectively.

In addition to the quantitative approach for the estimation of the pavement stiffness modulus, a qualitative procedure is further developed. The investigated road stretch is divided into 50m-long value ranges of stiffness modulus, wherein the average value is taken as a benchmark. Three classes of pavement stiffness (i.e., “high stiffness”, “medium stiffness” and “low stiffness”) are therefore set based on two arbitrarily-fixed threshold values. These are selected according to the overall trend

462 of modelled stiffness moduli and allow for customisation of the methodology as per the specific  
463 requirements of the survey.

464 The model viability is finally evaluated by quantitative and qualitative comparison of measured and  
465 modelled stiffness moduli. The quantitative analysis of the outputs shows a value of the normalised  
466 root-mean-square deviation (NRMSD) equal to 0.273. Hence, a relatively good agreement between  
467 measured and modelled data is proven. This outcome is also confirmed by the quantitative analysis,  
468 whereby good matches of the defined stiffness classes are found across the whole investigated road  
469 stretch.

470 It is important to emphasize the importance of the proposed methodology for extensive and time-  
471 efficient assessment of roads at the network level and potential implementation in pavement  
472 management systems (PMS). This could be crucial for road administrators and agencies in order to  
473 define priorities of intervention, allocate costs effectively and decrease the likelihood of envisaged  
474 accidents.

475 Future research could task itself with enriching the database for the development of the proposed  
476 methodology with a larger data sample from different road sections. In addition, different sources of  
477 ground-truth data for collection of stiffness moduli (e.g. falling weight deflectometer, curviameter,  
478 traffic speed deflectometer) could be used for the investigation of deeper domains and/or the  
479 gathering of more dense data. Comparison of model outputs against the actual strength and  
480 deformation data would allow for the understanding of the viability of different ground-truth  
481 equipment for modelling purposes.

## 482 **Acknowledgements** 483

484 The authors express their thanks to Mr. Spartaco Cera, from Roma Tre University, for technical  
485 assistance during the survey. Special thanks to IDS Georadar for supplying the GPR antenna  
486 system. This work has also benefited from the network activities carried out within the EU funded



487 COST Action TU1208 “Civil Engineering Applications of Ground Penetrating Radar.”

488

489 **References**

- 490 1. S.–P. Miaou, The relationship between truck accidents and geometric design of road sections:  
491 Poisson versus negative binomial regressions, *Accident Anal. Prev.* 26 (4) (1994) 471–482.
- 492 2. P.C. Anastatoupulos, A.P. Tarko, F.L. Mannering, Tobit analysis of vehicle accident rates on  
493 interstate highways, *Accident Anal. Prev.* 40 (2) (2008) 768–775.
- 494 3. S. Tighe, N. Li, L.C. Falls, R. Haas, Incorporating road safety into pavement management,  
495 *Transp. Res. Rec.* 1699 (2000) 1–10.
- 496 4. ASTM D1195/D1195M-09, Standard test method for repetitive static plate load tests of soils and  
497 flexible pavement components, for use in evaluation and design of airport and highway  
498 pavements, ASTM International, West Conshohocken, PA., 2009.
- 499 5. ASTM D4695-03, Standard Guide for General Pavement Deflection Measurements, ASTM  
500 International, West Conshohocken, PA, 2008.
- 501 6. ASTM D4429-09a, Standard Test Method for CBR (California Bearing Ratio) of Soils in Place”,  
502 ASTM International, West Conshohocken, PA, 2009.
- 503 7. ASTM D4694-09, Standard Test Method for Deflections with a Falling- Weight-Type Impulse  
504 Load Device”, ASTM International, West Conshohocken, PA., 2009.
- 505 8. ASTM E2583-07, Standard Test Method for Measuring Deflections with a Light Weight  
506 Deflectometer (LWD)”, ASTM International, West Conshohocken, PA., 2011.
- 507 9. A. Benedetto, F. Tosti, L. Di Domenico, Elliptic model for prediction of deflections induced by a  
508 Light Falling Weight Deflectometer. *J. Terramechanics* 49 (1) (2012) 1–12.
- 509 10. P.R. Fleming, M.W. Frost, J.P. Lambert, Review of lightweight deflectometer for routine in  
510 situ assessment of pavement material stiffness, *Transp. Res. Rec.*, (2007) 80–87
- 511 11. A. Benedetto, L. Pajewski, Eds. (2015), *Civil Engineering Applications of Ground*  
512 *Penetrating Radar*, Springer - Book Series: Springer Transactions in Civil and Environmental

- 513 Engineering; doi: 10.1007/978-3-319-04813-0
- 514 12. J.-M. Simonin, J.-L. Geffard, P. Hornych, Performance of deflection measurement  
515 equipment and data interpretation in France, International Symposium Non-Destructive Testing  
516 in Civil Engineering (NDT-CE) September 15–17, 2015, Berlin, Germany.
- 517 13. A. Zofka, J. Sudyka, Traffic speed deflectometer (TSD) measurements for pavement  
518 evaluation, in Proc. of the International Symposium on Non-Destructive Testing in Civil  
519 Engineering (NDT-CE), Berlin, Germany, Sept. 15–17, 2015.
- 520 14. A. Zofka, M. Graczyk, J. Rafa, Qualitative evaluation of stochastic factors affecting the Traffic  
521 Speed Deflectometer results, in Proc. of the Transportation Research Board 94<sup>th</sup> Annual  
522 Meeting, Washington DC, USA, Jan. 11–15, 2015.
- 523 15. C. Bruschini, B. Gros, F. Guerne, P.-Y. Pièce, O. Carmona, Ground penetrating radar and  
524 imaging metal detector for antipersonnel mine detection, J. Appl. Geophys. 40 (1-3) (1998) 59–  
525 71.
- 526 16. D. Goodman, Ground-penetrating radar simulation in engineering and archaeology,  
527 Geophysics, 59 (2), (1994) 224–232.
- 528 17. A.K. Benson, Applications of ground penetrating radar in assessing some geological  
529 hazards: examples of groundwater contamination, faults, cavities, J. Appl. Geophys. 33 (1-3)  
530 (1992) 177–193.
- 531 18. L.A. Plewes, B. Hubbard A review of the use of radio-echo sounding in glaciology, Progress  
532 in Physical Geography, 25 (2) (2001) 203–236.
- 533 19. F. Tosti, S. Adabi, L. Pajewski, G. Schettini, A. Benedetto, Large-scale analysis of dielectric  
534 and mechanical properties of pavement using GPR and LFWD, in Proc. of the 15th International  
535 Conference on Ground Penetrating Radar, Brussels, Belgium, Jun.-July 2014, pp. 868–873.
- 536 20. D.J. Daniels, Ground Penetrating Radar, IEEE Radar, Sonar, Navigation and Avionics Ed.,  
537 2006.

- 538 21. D.G. Fredlung, H. Rahardjo, M.D. Fredlung, *Unsaturated Soil Mechanics in Engineering*  
539 *Practice*, Jhon Wiley & Sons Ed., 2012.
- 540 22. J.K. Mitchell, *Fundamentals of Soil Behaviour*, Second Edition. John Wiley & Sons Ed.,  
541 1993.
- 542 23. S.H. Carpenter, R.L. Lytton, J.A. Epps, Pavement cracking in west texas due to freeze-thaw  
543 cycling, *Transp. Res. Rec.*, 532 (1975) 1–13.
- 544 24. T. Scullion, T. Saarenketo, Using suction and dielectric measurements as performance  
545 indicators for aggregate base materials, *Transp. Res. Rec.*, 1577 (1997) 37–44.
- 546 25. T. Saarenketo, The use of dielectric and electrical conductivity measurements and ground  
547 penetrating radar for frost susceptibility evaluations of subgrade soils, in *Proc. of the Symposium*  
548 *on the Application of Geophysics to Engineering and Environmental Problems (SAGEEP) 95*,  
549 1995, pp. 73–85.
- 550 26. A. S. Noureldin, K. Zhu, S. Li, D. Harris, Network pavement evaluation using falling weight  
551 deflectometer and ground penetrating radar, *Transp. Res. Rec.*, 1860 (1) 765–797.
- 552 27. Y.H. Huang, *Pavement Analysis and Design*, Prentice-Hall Ed., 2004.
- 553 28. E. Tutumler, D.S. Little, S.-H. Kim, A validated model for predicting field performance of  
554 aggregate base courses, in *Proc. of the 82nd Annual Meeting of the Transportation Research*  
555 *Board*, Washington, DC, 2003.
- 556 29. R. Horn, Strength of structured soils due to loading- a review of the processes on macro-  
557 and microscale-European aspects. In: Larson WE, Blake GR, Allmaras RR, Voorhees WB,  
558 Gupta S, editors. *Mechanics and related processes in structured agricultural soils*. Kluwer Publ;  
559 *Applied Sciences*; 1989. pp. 9–22.
- 560 30. D.M. Burmister, The general theory of stresses and displacements in layered systems, *J.*  
561 *Appl. Phys.*, 16, 126 (1945) (2004).
- 562 31. C.R. Foster, R.G. Ahlvin, Stresses and deflections induced by a uniform circular load, in  
563 *Proc. of Highway Research Board*, 33 (1954) 467–470.

- 564 32. M. Novak, B. Birgisson, R. Roque, Near-surface stress states in flexible pavements using  
565 measured radial tire contact stresses and ADINA, *Comput. Struct.*, 81 (2003) 859–870.
- 566 33. S. Oteng-Seifah, P. G. Manke, Study of Rutting in Flexible Highway Pavements in  
567 Oklahoma (Abridgment), *Transp. Res. Record*, 602 (1976) 97–99.
- 568 34. A.L. Simpson, J.F. Daleiden, W.O. Hadley (1995) Rutting Analysis from a Different  
569 Perspective, *Transp. Res. Rec.*, 1473, 9-17.
- 570 35. C. Plati, A. Loizos, Estimation of in-situ density and moisture content in HMA pavements  
571 based on GPR trace reflection amplitude using different frequencies, *J. Appl. Geophys.*, 97  
572 (2013) 3–10.
- 573 36. F. Tosti, C. Patriarca, E. Slob, A. Benedetto, S. Lambot, Clay content evaluation in soils  
574 through GPR signal processing, *J. Appl. Geophys.*, 97 (2013) 69-80.
- 575 37. F. Tosti, A. Benedetto, L. Bianchini Ciampoli, S. Lambot, C. Patriarca, E. Slob, GPR  
576 analysis of clayey soil behaviour in unsaturated conditions for pavement engineering and  
577 geoscience applications, *Near Surf. Geophys.*, 14(2) (2016) 127-144.
- 578 38. H. Jol (Ed.), *Ground Penetrating Radar*, Elsevier, 2009.
- 579 39. P. Ullidtz (Ed.), *Pavement Analysis*, Elsevier, 1987.
- 580 40. S. Baltzer, J.M. Jansen, Temperature correction of asphalt-moduli for FWD measurements,  
581 in *Proc. of the 4th International Conference on the Bearing Capacity of Roads and Airfields*  
582 *(BCRRA)*, University of Minneapolis, Minnesota, July 17 -21, 1994, pp. 7–25.
- 583 41. A. Benedetto, F. Tosti, L. Bianchini Ciampoli, F. D’Amico, An overview of ground-  
584 penetrating radar signal processing techniques for road inspections, *Signal Process.*, 132 (2016)  
585 201–209.
- 586 42. I.L. Al-Qadi, S. Lahouar, Measuring layer thicknesses with GPR – Theory to practice,  
587 *Constr. Build. Mater.*, 19 (2005) 763–772.
- 588 43. ISPRA – Istituto Superiore per la Protezione e la Ricerca Ambientale -  
589 <http://sgi.isprambiente.it/geoportal/catalog/sgilink/map100k.page> (retrieved 22 Jun. 2017).